

On Sample-Efficient Generalized Planning via Learned Transition Models

Nitin Gupta*, Vishal Pallagani*, John A. Aydin, Biplav Srivastava

University of South Carolina
 {niting@email., vishalp@email., jaaydin@email., biplav}@sc.edu

Abstract

Generalized planning studies the construction of solution strategies that generalize across families of planning problems sharing a common domain model, formally defined by a transition function $\gamma : S \times A \rightarrow S$. Classical approaches achieve such generalization through symbolic abstractions and explicit reasoning over γ . In contrast, recent Transformer-based planners, such as PlanGPT and Plansformer, largely cast generalized planning as direct action-sequence prediction, bypassing explicit transition modeling. While effective on in-distribution instances, these approaches typically require large datasets and model sizes, and often suffer from state drift in long-horizon settings due to the absence of explicit world-state evolution. In this work, we formulate generalized planning as a transition-model learning problem, in which a neural model explicitly approximates the successor-state function $\hat{\gamma} \approx \gamma$ and generates plans by rolling out symbolic state trajectories. Instead of predicting actions directly, the model autoregressively predicts intermediate world states, thereby learning the domain dynamics as an implicit world model. To study size-invariant generalization and sample efficiency, we systematically evaluate multiple state representations and neural architectures, including relational graph encodings. Our results show that learning explicit transition models yields higher out-of-distribution satisficing-plan success than direct action-sequence prediction in multiple domains, while achieving these gains with significantly fewer training instances and smaller models. **This is an extended version of a short paper accepted at ICAPS 2026 under the same title.**

Code —

<https://github.com/ai4society/state-centric-gen-planning>

Introduction

Classical automated planning is defined over a state-transition system $\Sigma = \langle S, A, \gamma \rangle$, where S is the set of states, A the set of actions, and $\gamma : S \times A \rightarrow S$ the transition function. A planning task $\Pi = \langle \Sigma, s_0, g \rangle$ consists of an initial state $s_0 \in S$ and a goal condition g , typically represented as a set of literals such that a state s satisfies g iff $g \subseteq s$. A solution is an action sequence $\pi = \langle a_1, \dots, a_n \rangle$ such that

$s_{t+1} = \gamma(s_t, a_t)$ and the final state s_n satisfies g . Generalized planning seeks strategies that solve families of such tasks sharing a common γ .

Recent learning-based approaches to generalized planning predominantly model the conditional distribution $p(\pi | \Pi)$, for example via an autoregressive factorization $p(\pi | \Pi) = \prod_{t=1}^T p(a_t | \Pi, a_{<t})$ or a policy $\pi_\theta(a_t | s_t, g)$, and directly predict action sequences from problem descriptions, as in Plansformer (Pallagani et al. 2022), PlanGPT (Rossetti et al. 2024b), and symmetry-aware Transformers (Fritzsche, Gestrin, and Seipp 2025). This action-centric formulation bypasses explicit modeling of γ : the evolving world state s_t is never directly represented, and long-horizon reasoning relies on implicit correlations between action tokens, leading to state drift in out-of-distribution regimes.

In this work, we instead model generalized planning as a transition-model learning problem. Rather than predicting the next action, we learn a goal-conditioned neural transition model \mathcal{T}_θ that predicts the successor state along a plan trajectory, i.e., given the current state s_t and goal g (or problem description Π), the model outputs a prediction $\hat{s}_{t+1} = \mathcal{T}_\theta(s_t, g)$. Plans are then obtained by rolling out the predicted state trajectory and recovering the corresponding actions via local symbolic search over applicable operators, by matching $\gamma(s_t, a)$ to \hat{s}_{t+1} . This formulation enforces explicit world-state evolution, enables successor validation, and constrains learning to respect frame axioms and causal effects. It is consistent with model-based world modeling in reinforcement learning (Ha and Schmidhuber 2018; Hafner et al. 2019), but applied here to symbolic generalized planning.

For clarity, we refer to methods that directly predict actions (e.g., modeling $p(\pi | \Pi)$ or $\pi_\theta(a_t | s_t, g)$) as *action-centric* learning, and to methods that predict successor states via $\mathcal{T}_\theta(s_t, g)$ as *state-centric* learning. This usage is distinct from heuristic-based state-space learning in existing GP taxonomies (Chen, Trevizan, and Thiébaux 2025) and serves only to distinguish transition-model learning from direct action modeling.

A central challenge in learning \mathcal{T}_θ for GP is size invariance: the description of a state in S scales with the number of objects. To address this, we systematically evaluate multiple fixed-dimensional state representations, including fixed-size factored encodings and Weisfeiler–Leman (WL) graph

*These authors contributed equally.

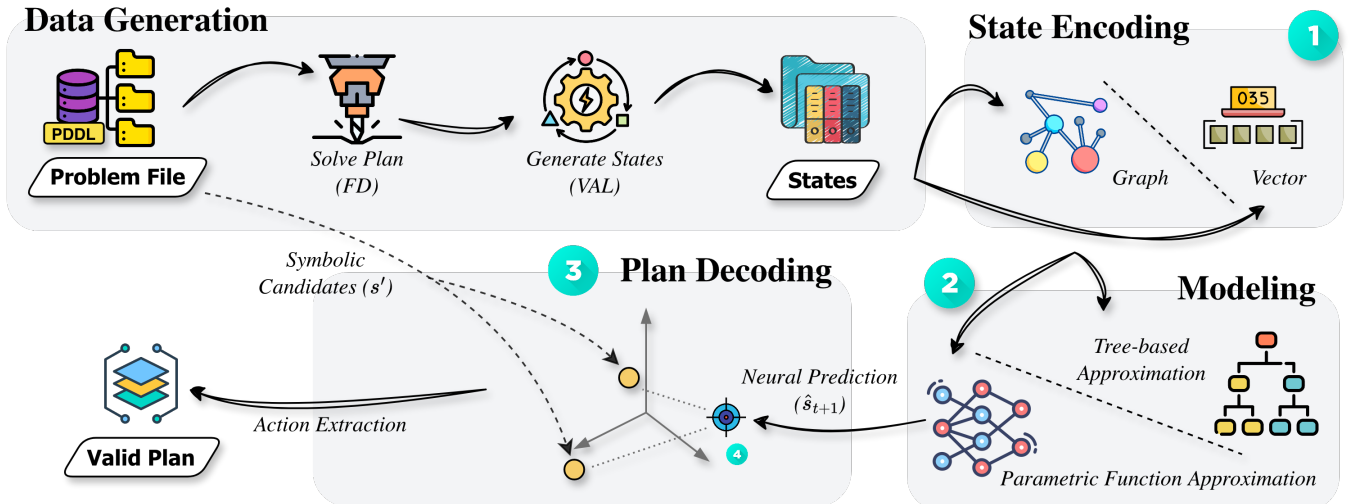


Figure 1: **State-Centric Generalized Planning Pipeline.** From a symbolic planning instance Π , executable plans are generated using a learned transition model. **(1) State Encoding:** Symbolic state–goal pairs (s_t, g) are mapped to fixed-dimensional embeddings $\phi(s_t)$ using either WL graph kernels or fixed-size factored vectors. **(2) Transition Modeling:** A parametric model (LSTM) or a non-parametric model (XGBoost) learns residual state transitions Δ_t to predict successor embeddings. **(3) Neuro-Symbolic Plan Decoding:** The predicted successor embedding $\hat{\phi}(s_{t+1})$ is matched against all valid symbolic successors $\text{Succ}(s_t)$ induced by γ , and the nearest valid successor is selected to recover the executable action. This guarantees symbolic validity while enabling transition-model-based generalization.

embeddings (Chen, Trevizan, and Thiébaux 2024). WL embeddings map variable-sized relational states to fixed-length structural feature vectors, enabling compact models such as LSTMs (Hochreiter and Schmidhuber 1997) and XGBoost (Chen 2016) to generalize from small to large problem instances. We empirically show that relational WL features are critical for size-invariant and sample-efficient generalization. Our contributions, thus, are (i) a transition-model-based formulation of generalized planning via goal-conditioned successor-state prediction; (ii) a systematic evaluation of state representations for size-invariant and sample-efficient generalization; and (iii) an empirical demonstration that compact models achieve competitive GP performance with orders of magnitude fewer parameters and training instances than Transformer-based planners.

Related Work

Learning-based approaches to generalized planning seek policies or models that transfer across problem instances within a domain. Early neural GP work introduced relational inductive biases to enable size generalization, including Action Schema Networks (Toyer et al. 2018) and graph-based deep RL for Blocksworld (Rivlin, Hazan, and Karpas 2020), as well as finite-state policy representations (Ståhlberg, Bonet, and Geffner 2022). More recent work formulates GP as sequence prediction: Plansformer (Pallagani et al. 2022) and PlanGPT (Rossetti et al. 2024b) train Transformer architectures to directly generate action sequences, while symmetry-aware Transformers (Fritzsche, Gestrin, and Seipp 2025) introduce architectural and contrastive constraints to improve permutation invariance. How-

ever, such action-centric models do not explicitly learn transition dynamics and often exhibit state drift under distributional shift. In parallel, graph-based state representations have been extensively studied for learning heuristics and value functions in planning, including STRIPS-HGN (Shen, Trevizan, and Thiébaux 2020), GOOSE (Chen, Thiébaux, and Trevizan 2023), and domain-independent graph transformations (Chen and Thiébaux 2024). Recent work shows that Weisfeiler–Leman (WL) graph kernels combined with lightweight regressors can match or exceed GNN performance at far lower cost (Chen, Trevizan, and Thiébaux 2024; Chen 2025; Hao et al. 2025). Hybrid neuro-symbolic systems integrate learned components with symbolic solvers or validators, including LLM+P (Liu et al. 2023), symbolic validation for PlanGPT (Rossetti et al. 2024a), LLM-Modulo (Kambhampati et al. 2024), and Say-Can for robotics (Ahn et al. 2022). Separately, model-based reinforcement learning demonstrates the benefits of learning explicit world models for planning (Ha and Schmidhuber 2018; Hafner et al. 2019). In contrast to prior action-sequence and heuristic-centric neural planners, our work adopts a transition-prediction formulation of generalized planning with size-invariant state representations, enabling sample-efficient and robust out-of-distribution generalization using compact models. Extended discussion is in Appendix B.

Transition-Model-Based Generalized Planning

Figure 1 illustrates the complete pipeline of our approach, consisting of symbolic data generation, size-invariant state encoding, transition-model learning, and plan decoding via

symbolic verification.

Generalized Planning Setup. A planning instance is $\Pi = \langle \mathcal{O}, \mathcal{P}, \mathcal{A}, s_0, g \rangle$, where \mathcal{O} is a finite object set, \mathcal{P} a predicate vocabulary, \mathcal{A} a set of operators, $s_0 \subseteq \mathcal{P}(\mathcal{O})$ the initial state, and $g \subseteq \mathcal{P}(\mathcal{O})$ the goal condition. Operators induce a deterministic transition function $\gamma : S \times \mathcal{A} \rightarrow S$. A plan $\pi = \langle a_1, \dots, a_T \rangle$ satisfies $s_{t+1} = \gamma(s_t, a_t)$ and $g \subseteq s_T$. Generalized planning seeks a single parameterized model trained on instances from $\mathcal{D}_{\text{train}}$ (small $|\mathcal{O}|$) that generalizes to $\mathcal{D}_{\text{test}}$ with much larger $|\mathcal{O}|$.

Size-Invariant State Representation. Each state-goal pair (s, g) is encoded as a relational instance graph $G_{s,g}$ and embedded using k iterations of WL color refinement. Node color histograms yield a fixed-dimensional embedding $\phi(s, g) \in \mathbb{R}^D$, where D depends only on the domain and is independent of $|\mathcal{O}|$. We overload notation and write $\phi(s)$ and $\phi(g)$ for the state and goal components, respectively. The resulting representation is permutation-invariant, size-invariant, and as expressive as 1-WL message-passing GNNs while enabling lightweight downstream models.

State-Centric Transition-Model Learning. Rather than learning a policy $\pi_\theta(a_t | s_t, g)$, we learn a neural transition model $f_\theta : \mathbb{R}^D \times \mathbb{R}^D \rightarrow \mathbb{R}^D$ that predicts state updates in embedding space. We denote this embedding-space transition model as f_θ ; the conceptual model \mathcal{T}_θ from the introduction is realized as

$$\mathcal{T}_\theta(s_t, g) \approx \phi^{-1}(\phi(s_t) + f_\theta(\phi(s_t), \phi(g)))$$

where the inverse is approximated via nearest-neighbor decoding. To exploit the sparsity of STRIPS-style transitions, where most predicates remain unchanged, we adopt a residual formulation:

$$\hat{\phi}(s_{t+1}) = \phi(s_t) + f_\theta(\phi(s_t), \phi(g))$$

where f_θ predicts a delta vector Δ_t . This explicitly encodes frame axioms and improves sample efficiency, particularly for non-sequential models. We train by minimizing the squared error over expert trajectories:

$$\mathcal{L} = \sum_t \|\hat{\phi}(s_{t+1}) - \phi(s_{t+1})\|_2^2.$$

Plan Decoding via Neuro-Symbolic Verification. At test time, the true symbolic state s_t is maintained throughout execution. Given s_t , the transition model produces a target embedding $\mathbf{v}_t = \phi(s_t) + f_\theta(\phi(s_t), \phi(g))$. Using the symbolic operators, we enumerate all valid successors

$$\text{Succ}(s_t) = \{\gamma(s_t, a) \mid a \in \mathcal{A}, a \text{ applicable in } s_t\}$$

and select the successor whose embedding is closest to the neural prediction:

$$s_{t+1} = \arg \min_{s' \in \text{Succ}(s_t)} \|\phi(s') - \mathbf{v}_t\|_2.$$

The executed action is the unique a satisfying $\gamma(s_t, a) = s_{t+1}$, which is well-defined under deterministic operators.

Algorithm 1: State-Centric GP with Plan Decoding

Require: Initial state s_0 , goal g , operators \mathcal{A} , learned model f_θ , embedding ϕ
Ensure: Valid plan π
1: $t \leftarrow 0, \pi \leftarrow \langle \rangle, s_t \leftarrow s_0$
2: **while** $g \not\subseteq s_t$ **do**
3: $\mathbf{v}_t \leftarrow \phi(s_t) + f_\theta(\phi(s_t), \phi(g))$
4: $\text{Succ}(s_t) \leftarrow \{\gamma(s_t, a) \mid a \in \mathcal{A}, a \text{ applicable in } s_t\}$
5: $s_{t+1} \leftarrow \arg \min_{s' \in \text{Succ}(s_t)} \|\phi(s') - \mathbf{v}_t\|_2$
6: $a_t \leftarrow \text{unique } a \text{ such that } \gamma(s_t, a) = s_{t+1}$
7: $\pi.\text{append}(a_t), s_t \leftarrow s_{t+1}, t \leftarrow t + 1$
8: **end while**
9: **return** π

This decoding step guarantees symbolic validity at every timestep and performs online correction of neural prediction errors. The procedure terminates when $g \subseteq s_t$. The full planning algorithm is summarized in Algorithm 1.

Experimental Setup

We evaluate whether learning an explicit transition model enables sample-efficient and size-invariant generalized planning. Our experiments assess (i) extrapolative out-of-distribution (OOD) generalization from small to large instances, (ii) whether parametric function approximation is necessary for learning transition dynamics, and (iii) the impact of size-invariant state representations.

Domains and Data. We evaluate on 4 IPC benchmark domains: *Blocksworld*, *Gripper*, *Logistics*, and *VisitAll*. Problem instances are sourced from the Symmetry-Aware Transformer repository, following the same data splits for fair comparison. Symbolic plans are generated using Fast Downward (Helmert 2006) with the landmark-cut heuristic, and complete state trajectories are reconstructed using VAL (Howey, Long, and Fox 2004). Data is partitioned into four splits by object count: *Training* (small instances, e.g., 4–7 blocks), *Validation* (similar or slightly larger sizes, held out), *Interpolation* (unseen configurations within the training size range), and *Extrapolation* (strictly larger than any training instance, e.g., 9–17 blocks). Extrapolation is the primary evaluation axis for size-invariant generalized planning. Full dataset statistics are reported in Appendix section D.

State Representations. We compare WL graph embeddings (Chen and Thiébaux 2024), which are permutation- and size-invariant, against Fixed-Size Factored (FSF) encodings. FSF encodings represent states as fixed-dimensional vectors with pre-assigned object slots, deliberately omitting the relational structure of WL to isolate the contribution of invariant representations to OOD generalization (Boutillier, Dearden, and Goldszmidt 2000; Guestrin et al. 2003). Details about both representations are in Appendix sections E and F.

Transition Models. We evaluate two transition-model classes: a parametric neural model (two-layer LSTM) and a tree-based, nonparametric regressor (XGBoost). The LSTM

tests whether sequential memory is necessary for trajectory-level transition dynamics, while XGBoost tests whether a local approximation of the transition kernel suffices. This comparison isolates the role of temporal memory. Both models are trained in state-prediction and delta-prediction modes, as defined in previous sections. The entire technical pipeline and hyperparameters are reported in Appendix section G.

Baselines. We compare against published results from Symmetry-Aware Transformers (SATr), which include results on PlanGPT, including applicability-filtered and re-grounded variants. We further run inference with Plansformer on our test instances using its publicly released checkpoint; it was trained on Blocksworld but not on Gripper, Logistics, or VisitAll, so its zero-shot cross-domain performance is expected to be limited. PlanGPT results are taken directly from Fritzsche, Gestrin, and Seipp (2025), who train and evaluate PlanGPT on the same data splits and counts as SATr; the weak interpolation/extrapolation performance reflects the difficulty of learning generalized policies from small training sets via action-centric sequence prediction. As a symbolic upper bound, we include Fast Downward with A* and the landmark-cut heuristic. While alternative configurations such as LAMA (Richter and Westphal 2010) may improve coverage on extrapolation instances at varying runtimes, we retain A*+LM-cut as a fixed reference; the neural baselines serve primarily to compare learning paradigms rather than to benchmark against optimized classical planners.

Inference and Metrics. At test time, plans are generated using the neuro-symbolic decoding procedure in Algorithm 1 with beam width 3 and a horizon cap of 100. Performance is measured by *satisficing success rate*, i.e., the fraction of instances for which a generated plan is valid under the transition model and reaches a goal state within the horizon limit, as verified by VAL. We additionally report changes in satisficing success across successive rollouts (seeds) to quantify stability under repeated decoding.

Results and Analysis

Table 1 reports satisficing-plan success rates across all domains, splits, representations, model classes, and prediction modes. The primary empirical finding is that explicit transition-model learning combined with size-invariant relational representations yields stronger or matching extrapolation than action-centric sequence prediction in domains with locally factored domains, while remaining insufficient for the Logistics benchmark under strict size extrapolation.

Comparison with action-centric planners. Under strict extrapolation, Plansformer and all PlanGPT variants achieve 0.00 success across all four domains. Plansformer further exhibits 0.00 on non-Blocksworld domains since they are not present in its training data. SATr attains non-zero extrapolation in Blocksworld (0.13), Gripper (0.79), and VisitAll (0.64), but fails in Logistics. The best state-centric models exceed SATr in Blocksworld (WL-XGB delta 0.45 vs.

0.13) and VisitAll (0.87 vs. 0.64), while SATr remains superior in Gripper extrapolation (0.79 vs. 0.25). Notably, these gains are obtained using compact transition models trained on unaugmented state trajectories: our LSTM has $\sim 1\text{M}$ parameters and XGBoost $\sim 115\text{K}$ tree nodes, compared to $\sim 25\text{--}35\text{M}$ (SATr), $\sim 125\text{M}$ (PlanGPT), and $\sim 220\text{M}$ (Plansformer). Furthermore, SATr augments training data via symmetry-based state-space expansion, whereas our models are trained on the original small training sets without any augmentation (e.g., 9 instances in Blocksworld). This indicates that, under appropriate relational abstractions, explicit transition learning can match or exceed extrapolation at orders-of-magnitude lower model and data cost, suggesting that learning domain physics provides a stronger inductive bias for generalization than architectural scale or data augmentation alone. A detailed breakdown of parameter counts and training data requirements is provided in Appendix section C.2.

Effect of size-invariant relational representations.

Across all domains, FSF-based encodings yield negligible extrapolation performance: Blocksworld (0.00), Gripper (0.00), VisitAll (≤ 0.13), and Logistics (0.00). In contrast, WL-based models achieve strictly positive extrapolation in three domains. In Blocksworld, WL-XGB (delta) reaches 0.45 compared to 0.00 for all FSF variants. In VisitAll, WL-XGB (delta) reaches 0.87 while FSF-XGB (delta) reaches only 0.13. This establishes that extrapolation beyond the training object bound requires a permutation- and size-invariant abstraction $\phi : S \rightarrow \mathbb{R}^D$. Fixed-slot encodings restrict the hypothesis class to a bounded object universe and therefore fail when $|\mathcal{O}|_{\text{test}} > |\mathcal{O}|_{\text{train}}$.

Effect of residual transition modeling. For tree-based models, residual parameterization consistently improves extrapolation. In Blocksworld, WL-XGB improves from 0.25 (state) to 0.45 (delta). In VisitAll, it improves from 0.08 to 0.87. This behavior is consistent with STRIPS transition semantics, $\gamma(s, a) = (s \setminus \text{Del}(a)) \cup \text{Add}(a)$, which induces sparse state differences. The delta formulation constrains learning to the subspace of changed fluents, reducing regression variance for non-parametric models. For LSTM, the effect is domain dependent: delta improves Blocksworld extrapolation (0.03 \rightarrow 0.15) but degrades Gripper (0.25 \rightarrow 0.17), indicating interaction between residual bias and recurrent state memory.

Sequential versus non-sequential transition learning.

Comparing WL-LSTM and WL-XGB isolates the role of temporal memory. In Gripper extrapolation, WL-LSTM (state) attains 0.25 while both XGB variants remain at 0.00, indicating that under the chosen abstraction the induced transition kernel $P(\phi(s_{t+1}) \mid \phi(s_t), \phi(g))$ is not well-approximated by a purely local regressor. In contrast, in Blocksworld and VisitAll, WL-XGB (delta) outperforms WL-LSTM: Blocksworld (0.45 vs. 0.15) and VisitAll (0.87 vs. 0.59), indicating that the Markovian assumption, where the future depends only on the present state and not history, suffices under relational abstraction in these domains.

Table 1: Coverage rates (%) across all configurations. Values are reported as $Mean \pm Std$. Best result per row (over all non-FD configurations) is **bolded**, second best is underlined. Light gray columns denote our state-centric implementations. FD = Fast Downward (60s timeout). *Results from Fritzsche, Gestrin, and Seipp (2025).

Domain	Split	FD	Plansf.	PlanGPT*			SATr (enc)*		SATr (enc-dec)*			WL-LSTM		WL-XGB		FSF-LSTM		FSF-XGB	
		greedy	appl.	regr.	greedy	greedy	appl.	regr.	state	delta	state	delta	state	delta	state	delta	state	delta	
Blocks	Val.	1.00	1.00 _{±0.00}	0.00 _{±0.00}	0.00 _{±0.00}	0.00 _{±0.00}	1.00 _{±0.00}	1.00 _{±0.00}	1.00 _{±0.00}	1.00 _{±0.00}	<u>0.56</u> _{±0.16}	<u>0.67</u> _{±0.00}	1.00 _{±0.00}	<u>0.67</u> _{±0.00}	0.00 _{±0.00}	0.00 _{±0.00}	0.00 _{±0.00}	0.00 _{±0.00}	0.00 _{±0.00}
	Interp.	1.00	1.00 _{±0.00}	0.56 _{±0.16}	0.56 _{±0.16}	0.00 _{±0.00}	1.00 _{±0.00}	1.00 _{±0.00}	1.00 _{±0.00}	1.00 _{±0.00}	0.56 _{±0.16}	<u>0.89</u> _{±0.16}	1.00 _{±0.00}	1.00 _{±0.00}	0.00 _{±0.00}	0.00 _{±0.00}	0.00 _{±0.00}	0.00 _{±0.00}	0.00 _{±0.00}
	Extrap.	0.60	0.10 _{±0.00}	0.00 _{±0.00}	0.00 _{±0.00}	0.00 _{±0.00}	0.05 _{±0.07}	0.07 _{±0.02}	0.13 _{±0.05}	0.00 _{±0.00}	0.03 _{±0.02}	0.15 _{±0.07}	<u>0.25</u> _{±0.00}	0.45 _{±0.00}	0.00 _{±0.00}	0.00 _{±0.00}	0.00 _{±0.00}	0.00 _{±0.00}	0.00 _{±0.00}
Gripper	Val.	1.00	0.00 _{±0.00}	0.00 _{±0.00}	0.00 _{±0.00}	0.00 _{±0.00}	1.00 _{±0.00}	0.17 _{±0.24}	1.00 _{±0.00}	1.00 _{±0.00}	1.00 _{±0.00}	<u>0.67</u> _{±0.47}	0.00 _{±0.00}	0.00 _{±0.00}	0.17 _{±0.24}	0.33 _{±0.24}	0.00 _{±0.00}	0.00 _{±0.00}	
	Interp.	1.00	0.00 _{±0.00}	0.00 _{±0.00}	0.44 _{±0.16}	0.00 _{±0.00}	<u>0.89</u> _{±0.16}	0.67 _{±0.00}	1.00 _{±0.00}	1.00 _{±0.00}	1.00 _{±0.00}	<u>0.67</u> _{±0.47}	0.00 _{±0.00}	0.00 _{±0.00}	0.45 _{±0.32}	0.00 _{±0.00}	0.67 _{±0.00}	0.00 _{±0.00}	
	Extrap.	0.13	0.00 _{±0.00}	0.00 _{±0.00}	0.00 _{±0.00}	0.00 _{±0.00}	0.02 _{±0.03}	0.00 _{±0.00}	0.15 _{±0.06}	0.79 _{±0.16}	<u>0.25</u> _{±0.08}	0.17 _{±0.19}	0.00 _{±0.00}	0.00 _{±0.00}	0.08 _{±0.00}	0.00 _{±0.00}	0.00 _{±0.00}	0.00 _{±0.00}	
VisitAll	Val.	1.00	0.00 _{±0.00}	0.00 _{±0.00}	0.14 _{±0.12}	0.00 _{±0.00}	1.00 _{±0.00}	0.33 _{±0.09}	0.93 _{±0.04}	<u>0.99</u> _{±0.02}	<u>0.99</u> _{±0.02}	0.79 _{±0.29}	1.00 _{±0.00}	1.00 _{±0.00}	0.03 _{±0.04}	0.49 _{±0.02}	0.13 _{±0.00}	0.92 _{±0.00}	
	Interp.	1.00	0.00 _{±0.00}	0.05 _{±0.04}	0.67 _{±0.18}	0.41 _{±0.22}	1.00 _{±0.00}	0.87 _{±0.01}	<u>0.99</u> _{±0.01}	1.00 _{±0.00}	1.00 _{±0.00}	<u>0.99</u> _{±0.01}	1.00 _{±0.00}	1.00 _{±0.00}	0.56 _{±0.02}	0.38 _{±0.02}	0.86 _{±0.00}	0.95 _{±0.00}	
	Extrap.	0.50	0.00 _{±0.00}	0.00 _{±0.00}	0.02 _{±0.02}	0.00 _{±0.00}	0.42 _{±0.11}	0.00 _{±0.00}	0.15 _{±0.05}	<u>0.64</u> _{±0.12}	0.47 _{±0.05}	0.59 _{±0.40}	0.08 _{±0.00}	0.87 _{±0.00}	0.00 _{±0.00}	0.03 _{±0.01}	0.00 _{±0.00}	0.13 _{±0.00}	
Logistics	Val.	1.00	0.00 _{±0.00}	0.00 _{±0.00}	<u>0.08</u> _{±0.12}	0.00 _{±0.00}	0.00 _{±0.00}	0.00 _{±0.00}	0.00 _{±0.00}	0.00 _{±0.00}	0.00 _{±0.00}	<u>0.17</u> _{±0.12}	<u>0.08</u> _{±0.12}	0.00 _{±0.00}	0.00 _{±0.00}	0.00 _{±0.00}	0.00 _{±0.00}	0.00 _{±0.00}	
	Interp.	1.00	0.00 _{±0.00}	0.07 _{±0.05}	<u>0.44</u> _{±0.09}	0.19 _{±0.14}	0.11 _{±0.00}	0.22 _{±0.31}	0.26 _{±0.29}	0.22 _{±0.31}	0.78 _{±0.16}	0.29 _{±0.10}	0.11 _{±0.00}	0.00 _{±0.00}	0.18 _{±0.10}	0.11 _{±0.00}	<u>0.44</u> _{±0.00}	0.11 _{±0.00}	
	Extrap.	0.26	0.00 _{±0.00}	0.00 _{±0.00}	0.00 _{±0.00}	0.00 _{±0.00}	0.00 _{±0.00}	0.00 _{±0.00}	0.00 _{±0.00}	0.00 _{±0.00}	0.00 _{±0.00}	0.00 _{±0.00}	0.00 _{±0.00}	0.00 _{±0.00}	0.00 _{±0.00}	0.00 _{±0.00}	0.00 _{±0.00}	0.00 _{±0.00}	

Limitations under hierarchical causal coupling. All learned models, including all state-centric variants, achieve 0.00 extrapolation in *Logistics*. Even Fast Downward degrades from 1.00 (validation) to 0.26 (extrapolation) under a 60-second timeout, reflecting the exponential state-space growth of extrapolation instances. The *Logistics* domain exhibits deep multi-layer causal coupling across object types and transport modalities, which is not preserved under local successor matching. This identifies a concrete structural limitation of one-step neural transition prediction under strict size extrapolation for this domain.

Summary of empirical findings. The results support three data-grounded conclusions: (i) size-invariant relational representations are necessary for extrapolation beyond training object bounds; (ii) residual (delta) modeling significantly improves non-parametric transition learning in sparse STRIPS domains; and (iii) the necessity of sequential memory in transition learning is domain dependent. Transition-model learning alone, however, remains insufficient for hierarchical domains under strict extrapolation. An extended experimental analysis is presented in Appendix section C.

Conclusion and Future Work

We presented a state-centric formulation of generalized planning in which models learn to predict successor states rather than action sequences. When combined with size- and permutation-invariant relational embeddings, this approach enables compact transition models ($\sim 1M$ parameters, no data augmentation) to achieve strong extrapolation performance in locally factored domains, matching or exceeding Transformer baselines ($\sim 25\text{--}220M$ parameters) that rely on orders of magnitude more data and parameters. Empirically, our results show that explicit transition modeling provides a stronger inductive bias for extrapolation than architectural scale alone, though limitations remain in domains with hierarchical and long-range dependencies. The neuro-symbolic decoding interface further improves robustness by enforcing symbolic validity at every planning step. Future work will target hierarchical and long-range dependency domains, where one-step state prediction fails under strict extrapolation. We will extend the state-centric framework to multi-

step or abstract transitions while preserving symbolic verification.

Acknowledgments

This work is partially supported by NSF Awards #2454027 and NAIRR250014, and Faculty Award by JP Morgan Research.

References

- Ahn, M.; Brohan, A.; Brown, N.; Chebotar, Y.; Cortes, O.; David, B.; Finn, C.; Fu, C.; Gopalakrishnan, K.; Hausman, K.; et al. 2022. Do as i can, not as i say: Grounding language in robotic affordances. *arXiv preprint arXiv:2204.01691*.
- Battaglia, P. W.; Hamrick, J. B.; Bapst, V.; Sanchez-Gonzalez, A.; Zambaldi, V.; Malinowski, M.; Tacchetti, A.; Raposo, D.; Santoro, A.; Faulkner, R.; et al. 2018. Relational inductive biases, deep learning, and graph networks. *arXiv preprint arXiv:1806.01261*.
- Boutilier, C.; Dearden, R.; and Goldszmidt, M. 2000. Stochastic dynamic programming with factored representations. *Artificial intelligence*, 121(1-2): 49–107.
- Chen, D.; and Thiébaux, S. 2024. Graph learning for numeric planning. *Advances in Neural Information Processing Systems*, 37: 91156–91183.
- Chen, D. Z. 2024. WLPlan: Relational Features for Symbolic Planning. *CoRR*, abs/2411.00577.
- Chen, D. Z. 2025. Weisfeiler-Leman Features for Planning: A 1,000,000 Sample Size Hyperparameter Study. *arXiv preprint arXiv:2508.18515*.
- Chen, D. Z.; Thiébaux, S.; and Trevizan, F. 2023. Goose: Learning domain-independent heuristics. In *NeurIPS 2023 Workshop on Generalization in Planning*.
- Chen, D. Z.; Trevizan, F.; and Thiébaux, S. 2024. Return to tradition: Learning reliable heuristics with classical machine learning. In *Proceedings of the International Conference on Automated Planning and Scheduling*, volume 34, 68–76.
- Chen, D. Z.; Trevizan, F.; and Thiébaux, S. 2025. Learning for Generalised Planning. Tutorial, International Conference on Automated Planning and Scheduling (ICAPS). <https://l4p-tutorial.github.io/slides.pdf>.

- Chen, T. 2016. XGBoost: A Scalable Tree Boosting System. *Cornell University*.
- Fritzsche, M.; Gestrin, E.; and Seipp, J. 2025. Symmetry-Aware Transformer Training for Automated Planning. *arXiv preprint arXiv:2508.07743*.
- Guestrin, C.; Koller, D.; Parr, R.; and Venkataraman, S. 2003. Efficient solution algorithms for factored MDPs. *Journal of Artificial Intelligence Research*, 19: 399–468.
- Ha, D.; and Schmidhuber, J. 2018. World models. *arXiv preprint arXiv:1803.10122*, 2(3).
- Hafner, D.; Lillicrap, T.; Fischer, I.; Villegas, R.; Ha, D.; Lee, H.; and Davidson, J. 2019. Learning latent dynamics for planning from pixels. In *International conference on machine learning*, 2555–2565. PMLR.
- Hafner, D.; Pasukonis, J.; Ba, J.; and Lillicrap, T. 2023. Mastering diverse domains through world models. *arXiv preprint arXiv:2301.04104*.
- Hao, M.; Chen, D. Z.; Trevizan, F.; and Thiébaux, S. 2025. Effective data generation and feature selection in learning for planning. In *European Conference on Artificial Intelligence (ECAI-25)*.
- Helmert, M. 2006. The fast downward planning system. *Journal of Artificial Intelligence Research*, 26: 191–246.
- Hochreiter, S.; and Schmidhuber, J. 1997. Long short-term memory. *Neural computation*, 9(8): 1735–1780.
- Howey, R.; Long, D.; and Fox, M. 2004. VAL: Automatic plan validation, continuous effects and mixed initiative planning using PDDL. In *16th IEEE International Conference on Tools with Artificial Intelligence*, 294–301. IEEE.
- Kambhampati, S.; Valmееkam, K.; Guan, L.; Verma, M.; Stechly, K.; Bhambri, S.; Saldyt, L. P.; and Murthy, A. B. 2024. Position: LLMs can’t plan, but can help planning in LLM-modulo frameworks. In *Forty-first International Conference on Machine Learning*.
- Liu, B.; Jiang, Y.; Zhang, X.; Liu, Q.; Zhang, S.; Biswas, J.; and Stone, P. 2023. Llm+ p: Empowering large language models with optimal planning proficiency. *arXiv preprint arXiv:2304.11477*.
- Pallagani, V.; Muppasani, B.; Murugesan, K.; Rossi, F.; Horesh, L.; Srivastava, B.; Fabiano, F.; and Loreggia, A. 2022. Plansformer: Generating symbolic plans using transformers. *arXiv preprint arXiv:2212.08681*.
- Richter, S.; and Westphal, M. 2010. The LAMA planner: Guiding cost-based anytime planning with landmarks. *Journal of Artificial Intelligence Research*, 39: 127–177.
- Rivlin, O.; Hazan, T.; and Karpas, E. 2020. Generalized planning with deep reinforcement learning. *arXiv preprint arXiv:2005.02305*.
- Rossetti, N.; Tummolo, M.; Gerevini, A. E.; Olivato, M.; Putelli, L.; and Serina, I. 2024a. Enhancing GPT-based planning policies by model-based plan validation. In *International Conference on Neural-Symbolic Learning and Reasoning*, 328–337. Springer.
- Rossetti, N.; Tummolo, M.; Gerevini, A. E.; Putelli, L.; Serina, I.; Chiari, M.; and Olivato, M. 2024b. Learning general policies for planning through GPT models. In *Proceedings of the International Conference on Automated Planning and Scheduling*, volume 34, 500–508.
- Segovia-Aguas, J.; Jiménez, S.; and Jonsson, A. 2021. Generalized planning as heuristic search. In *Proceedings of the International Conference on Automated Planning and Scheduling*, volume 31, 569–577.
- Shen, W.; Trevizan, F.; and Thiébaux, S. 2020. Learning domain-independent planning heuristics with hypergraph networks. In *Proc. of the International Conference on Automated Planning and Scheduling*, volume 30, 574–584.
- Shervashidze, N.; Schweitzer, P.; Van Leeuwen, E. J.; Mehlhorn, K.; and Borgwardt, K. M. 2011. Weisfeiler-lehman graph kernels. *Journal of Machine Learning Research*, 12(9).
- Shlomi, E.; Azran, G.; Shapira, E.; Nahum, O.; Uziel, G.; Katz, M.; Tavor, A. A.; Reichart, R.; and Keren, S. 2025. Transition Function Prediction in AI Planning Using LLMs. In *AAAI 2025 Workshop LM4Plan*.
- Ståhlberg, S.; Bonet, B.; and Geffner, H. 2022. Learning generalized policies without supervision using gnns. *arXiv preprint arXiv:2205.06002*.
- Toyer, S.; Trevizan, F.; Thiébaux, S.; and Xie, L. 2018. Action schema networks: Generalised policies with deep learning. In *Proc. of the AAAI Conference on Artificial Intelligence*, volume 32.
- Weisfeiler, B.; and Leman, A. 1968. The reduction of a graph to canonical form and the algebra which appears therein. *nti, Series*, 2(9): 12–16.
- Xu, K.; Hu, W.; Leskovec, J.; and Jegelka, S. 2018. How powerful are graph neural networks? *arXiv preprint arXiv:1810.00826*.

Appendix

This appendix provides supplementary material to support reproducibility and extended analysis. It is organized as follows:

A. Notation and Terminology	7
B. Extended Related Work	7
C. Extended Experimental Analysis	9
D. Dataset Details and Statistics	9
E. Weisfeiler–Leman Graph Embedding Details	11
F. Fixed-Size Factored Encoding Details	12
G. Technical Implementation Pipeline	12

A Notation and Terminology

We summarize all symbols and technical terms used throughout the paper for clarity and reproducibility in Table 2.

B Extended Related Work

This section expands on the related work discussion in the main paper, providing additional context and citations for each research direction relevant to our work.

B.1 Learning for Generalized Planning

Generalized Planning (GP) seeks solution strategies that transfer across problem instances within a domain, rather than solving each instance independently (Segovia-Aguas, Jiménez, and Jonsson 2021). Early neural approaches introduced relational inductive biases to enable such transfer. Action Schema Networks (ASNs) (Toyer et al. 2018) exploited the lifted action structure of planning domains by constructing neural architectures that mirror action schemas, enabling policies to generalize beyond training instances. Rivlin, Hazan, and Karpas (2020) combined graph neural networks with deep reinforcement learning to learn Blocksworld policies that scale to instances orders of magnitude larger than those seen during training. These works established that an appropriate relational structure is critical for extrapolation in learned planners. More recent approaches have explored diverse architectural choices for GP. Ståhlberg, Bonet, and Geffner (2022) investigated learning general policies represented as finite-state controllers, providing theoretical grounding for the expressivity required for GP.

B.2 Symmetry and Invariance in Neural Planning

A fundamental challenge in neural planning is handling the symmetries inherent in planning problems: permuting object names should not change the solution structure. This has motivated architectures with explicit invariance properties. Graph Neural Networks (GNNs) naturally handle permutation invariance through message-passing operations (Battaglia et al. 2018).

The Symmetry-Aware Transformer (SATr) framework (Fritzsche, Gestrin, and Seipp 2025) addresses symmetry

in sequence-to-sequence planning. It introduces three innovations: compositional tokenization (separating objects and predicates), removal of positional encodings (preventing memorization of absolute positions), and contrastive learning objectives (encouraging mapping of symmetric states to similar representations). SATr achieves state-of-the-art performance on several IPC domains through extensive data augmentation (state-space expansion).

Our work differs from SATr in two fundamental respects. First, we adopt a *state-centric* rather than *action-centric* objective: predicting successor states rather than next actions. This forces the model to learn transition dynamics explicitly, providing natural grounding that architectural modifications alone cannot guarantee. Second, we achieve competitive generalization *without* massive data augmentation, relying instead on size-invariant representations (WL embeddings) that provide structural inductive bias.

B.3 Graph-Based State Representations

To handle variable-sized object sets, recent planners use graph-based state representations where objects are nodes and predicates define edges or features. Hypergraph networks such as STRIPS-HGN (Shen, Trevizan, and Thiébaux 2020) learned domain-independent heuristics directly from planning graphs. Chen, Thiébaux, and Trevizan (2023) proposed GOOSE, a GNN-based heuristic learner that significantly outperformed STRIPS-HGN and generalized to much larger problem instances. Subsequent work (Chen, Trevizan, and Thiébaux 2024) showed that classical Weisfeiler-Leman (WL) graph kernels (Weisfeiler and Leman 1968; Shervashidze et al. 2011) with simple regression models can match or exceed GNN performance at orders of magnitude lower computational cost. This finding motivates our use of WL embeddings: they provide the expressivity of 1-WL message-passing GNNs while enabling deployment with lightweight models.

Recent extensions have further improved graph-based representations for planning. Chen and Thiébaux (2024) introduced domain-independent graph transformations that enhance generalization, while Chen (2025) provided theoretical analysis connecting WL expressivity to planning-specific structures. Hao et al. (2025) demonstrated effective combinations of WL features with neural architectures for learning domain-independent heuristics.

B.4 Action-Centric Sequence Models for Planning

Another line of work formulates plan generation as a sequence prediction task. Plansformer (Pallagani et al. 2022) fine-tuned a Transformer on symbolic plan traces to generate action sequences with high validity on classical planning benchmarks, substantially outperforming zero-shot language models. More recently, PlanGPT (Rossetti et al. 2024b) trained GPT-style architectures directly on planning data to learn general planning policies. While effective in-distribution, such autoregressive models often suffer from state drift and logical inconsistency on longer horizons or out-of-distribution problems due to the lack of

Table 2: Summary of notation used throughout the paper.

Category	Symbol	Meaning
Planning	$\Sigma = \langle S, A, \gamma \rangle$	State-transition system (set of states S , actions A , and transition function γ)
	S	Set of all symbolic world states
	A, \mathcal{A}	Set of grounded actions (operators)
	$\gamma : S \times \mathcal{A} \rightarrow S$	Deterministic transition function
	\mathcal{O}	Finite object set in a planning instance
	\mathcal{P}	Predicate vocabulary
	$\mathcal{P}(\mathcal{O})$	Set of all grounded predicates over \mathcal{O}
	$s \subseteq \mathcal{P}(\mathcal{O})$	A symbolic state
	$\Pi = \langle \Sigma, s_0, G \rangle; \Pi = \langle \mathcal{O}, \mathcal{P}, \mathcal{A}, s_0, g \rangle$	Planning task (global and instance-level formulations)
Goals & Successors	s_0	Initial state of a planning instance
	$G \subseteq S$	Set of goal states in the state-transition formulation
	$g \subseteq \mathcal{P}(\mathcal{O})$	Goal condition in the propositional formulation
	$\text{Succ}(s)$	Set of valid symbolic successors of state s under γ
	$s_{t+1} = \gamma(s_t, a_t)$	Successor state obtained by applying action a_t in s_t
Learning & Transitions	$\mathcal{D}_{\text{train}}, \mathcal{D}_{\text{test}}$	Training and test distributions over planning instances
	\mathcal{T}_θ	Learned goal-conditioned transition model
	\hat{s}_{t+1}	Predicted successor state from \mathcal{T}_θ
	$\phi : S \rightarrow \mathbb{R}^D$	Fixed-dimensional state embedding
	$\phi(g)$	Embedded representation of the goal condition
	f_θ	Delta-prediction function in the residual transition parameterization
	Δ_t	Residual transition update at step t
	$\hat{\phi}(s_{t+1})$	Predicted next-state embedding, e.g., $\hat{\phi}(s_{t+1}) = \phi(s_t) + \Delta_t$
	\mathbf{v}_t	Target embedding used for decoding at step t
Decoding	$s_{t+1} = \arg \min_{s' \in \text{Succ}(s_t)} \ \phi(s') - \mathbf{v}_t\ _2$	Neuro-symbolic successor selection rule
	$a_t = \gamma^{-1}(s_t \rightarrow s_{t+1})$	Action inducing the selected symbolic transition
	T	Plan horizon (length of π)
	$\pi = \langle a_1, \dots, a_T \rangle$	Plan as an action sequence
Representations	WL	Weisfeiler–Leman (graph-kernel) state embedding
	FSF	Fixed-Size Factored state encoding
	ILG	Instance Learning Graph (relational encoding of (s, g))
	$G_{s,g}$	Relational instance graph encoding the pair (s, g)
	k	Number of WL refinement iterations
	D	Dimensionality of the embedding $\phi(s) \in \mathbb{R}^D$
Models	LSTM	Parametric recurrent transition model
	XGBoost (XGB)	Tree-based non-parametric regressor
	State mode	Direct prediction of $\phi(s_{t+1})$
	Delta mode	Prediction of residual Δ_t with reconstruction $\phi(s_t) + \Delta_t$
	θ	Trainable parameters of the learned models
	$\hat{\gamma}$	Learned approximation of the symbolic transition function γ
Evaluation	Validation / Interpolation / Extrapolation	Size-based dataset splits by object count
	Satisficing plan	Any valid plan whose execution reaches a goal state
	FD	Fast Downward planner (A* with LM-cut heuristic, 60s timeout)
	Coverage / Success rate	Fraction of test instances for which a satisficing plan is found

explicit state tracking. Concurrent work by Shlomi et al. (2025) explores LLM-based transition prediction from (s, a) pairs, but targets single-instance prediction rather than size-invariant generalized planning.

Hybrid LLM–Symbolic Planning. To mitigate these limitations, several hybrid frameworks integrate LLMs with symbolic planners or validators. LLM+P (Liu et al. 2023) uses an LLM to generate PDDL formulations that are solved by a classical planner, while recent PlanGPT variants incorporate symbolic validation to enforce action applicability (Rossetti et al. 2024a). Kambhampati et al. (2024) formalized this paradigm as *LLM-Modulo*, advocating tight coupling between LLMs and model-based solvers. In robotics, SayCan (Ahn et al. 2022) combines language models with learned affordance models to iteratively select feasible actions for long-horizon task execution.

Model-Based Learning and World Models. In reinforcement learning, learning explicit transition dynamics has proven beneficial for planning and generalization. World Models (Ha and Schmidhuber 2018) and subsequent model-based RL methods demonstrate that agents can learn compact environment simulators and plan via internal rollouts. However, most neural planners for classical planning remain action-centric or heuristic-driven and do not explicitly learn the symbolic transition dynamics. DreamerV3 (Hafner et al. 2023) extends world-model learning to diverse RL domains, motivating explicit dynamics modeling.

Positioning of Our Work. In contrast to prior action-sequence and heuristic-centric approaches, our work adopts a *state-centric, model-based learning* paradigm in which the planner is trained to predict state transitions directly. This enables explicit state grounding at every step, mitigates state drift, and yields significantly improved robustness on out-of-distribution instances using compact models. To the best of our knowledge, this transition-prediction formulation with size-invariant representations has not been previously explored for generalized neural planning.

C Extended Experimental Analysis

This section provides additional experimental analysis, including performance trends across problem sizes and per-problem breakdowns.

C.1 Performance Across Data Sets

Figures 2–4 show satisficing-plan success rate across different data splits, with plots showing the validation, interpolation, and extrapolation splits for each domain. These figures visualize the data presented in Table 1, providing a more intuitive view of performance trends across problem sizes and model configurations.

C.2 Model and Data Efficiency Analysis

A central empirical observation of this work is that explicit transition-model learning achieves competitive or superior extrapolation to action-centric Transformer baselines while requiring dramatically fewer parameters and training data.

This subsection provides detailed breakdowns supporting these claims.

Parameter Count Derivations. Table 3 summarizes model sizes across all methods. We detail the parameter calculations for our models below.

Table 3: Model size comparison across all methods. SATr estimates are derived from architectural specifications in Fritzsche, Gestrin, and Seipp (2025) (12-layer shared-weight encoder/decoder, hidden size 768); exact counts depend on domain-specific vocabulary embeddings, which are not reported in the SATr work.

Method	Parameters	Architecture	Ratio
Planformer	~220M	CodeT5	~230×
PlanGPT	~125M	GPT-2	~130×
SATr (enc–dec)	~25–35M	Transformer	~30×
Ours (LSTM)	~0.93M	2-layer LSTM	1×
Ours (XGB)	~115K nodes	Gradient boosting	—

LSTM parameter breakdown. The LSTM architecture comprises dual linear encoders ($D \rightarrow 32$), a two-layer LSTM (256-unit hidden size), and a two-stage output head ($256 \rightarrow 256 \rightarrow D$). The parameter count is dominated by the recurrent layers (~ 0.86 M) and scales linearly with the embedding dimension D . Across all experimental domains where D ranges from 412 to 723, the model contains between ~ 0.88 M and ~ 0.97 M trainable parameters, which we report as ~ 1 M.

XGBoost model size. XGBoost learns an ensemble of regression trees via gradient boosting. Model size is measured in total tree nodes across all boosting rounds and output dimensions. With a maximum depth of 8 and early stopping, typical models contain $\sim 115,000$ total nodes across all trees. Unlike neural models, XGBoost has no “trainable parameters” in the gradient-descent sense; the tree structure and leaf values are determined by the training algorithm.

D Dataset Details and Statistics

D.1 Domain Descriptions

We evaluate on four standard IPC benchmark domains that admit a classical STRIPS-style representation. Each domain is specified by a tuple $\langle \mathcal{O}, \mathcal{P}, \mathcal{A} \rangle$, where \mathcal{O} is the object set, \mathcal{P} is the predicate vocabulary, and \mathcal{A} is the operator set inducing a deterministic transition function $\gamma(s, a) = s \setminus \text{Del}(a) \cup \text{Add}(a)$. Detailed dataset statistics for each split are reported in Table 4.

Blocksworld. Blocksworld is a canonical manipulation domain defined over a set of blocks $\mathcal{O} = \{b_1, \dots, b_n\}$. The predicate set includes $\mathcal{P} = \{\text{on}(x, y), \text{ontable}(x), \text{clear}(x), \text{holding}(x), \text{handempty}\}$. The operator set \mathcal{A} consists of PICKUP, PUTDOWN, STACK, and UNSTACK. A state $s \subseteq \mathcal{P}(\mathcal{O})$ encodes a partial order over blocks. The branching factor grows quadratically in the number of clear blocks due to all admissible STACK/UNSTACK combinations. Transitions exhibit sparse

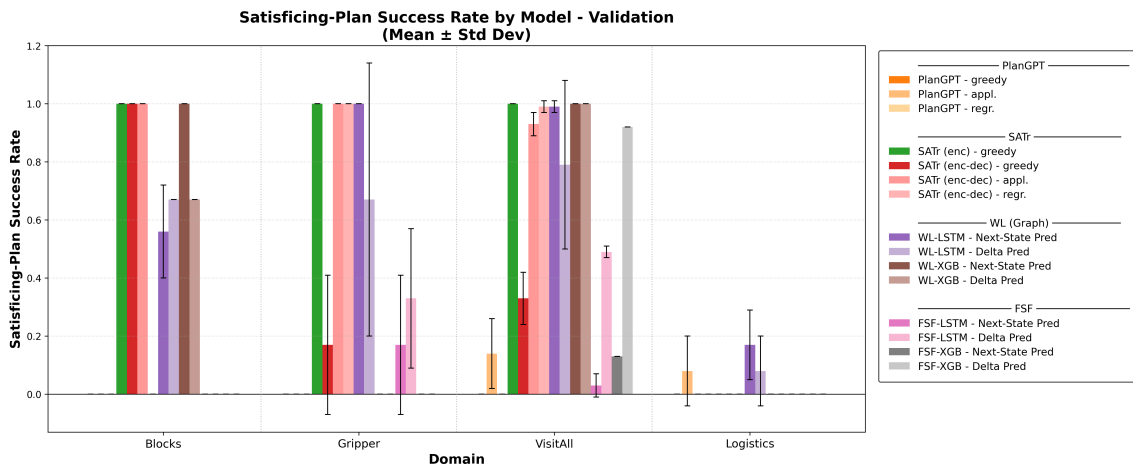


Figure 2: Satisficing-plan success rates on the validation split across all domains, comparing PlanGPT, SATr, WL-based, and FSF baselines.

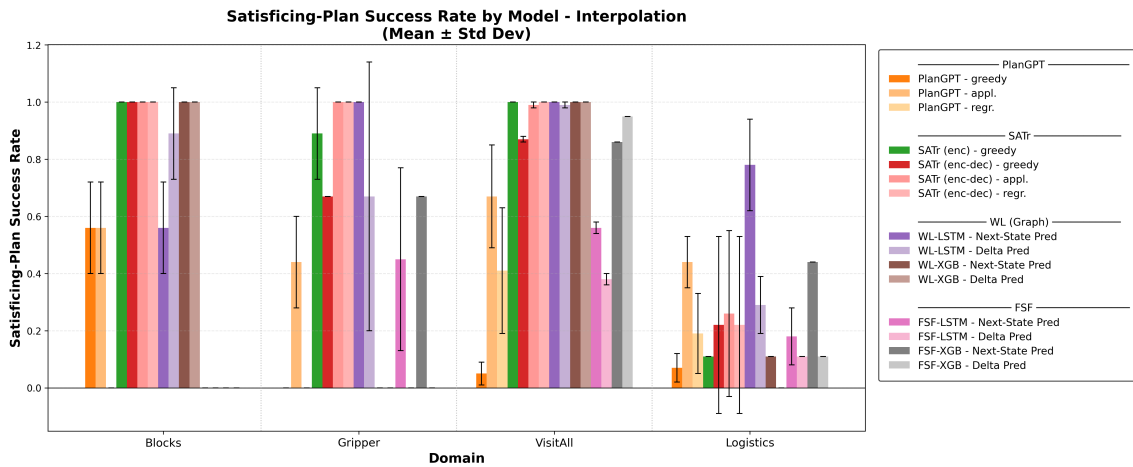


Figure 3: Satisficing-plan success rates on the interpolation split, comparing PlanGPT, SATr, WL-based, and FSF baselines for generalization to in-distribution problem instances.

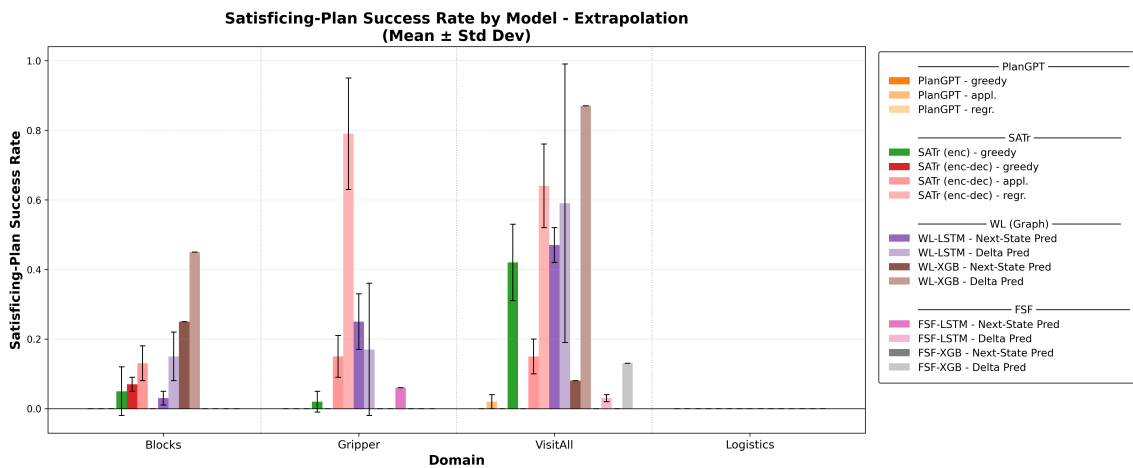


Figure 4: Satisficing-plan success rates on the extrapolation split, comparing PlanGPT, SATr, WL-based, and FSF baselines for generalization in out-of-distribution problem instances.

Table 4: Dataset statistics. Each cell shows *count (complexity values)* for the corresponding split. Complexity is measured in blocks, balls, goals, or cells depending on the domain. Training uses small instances; extrapolation tests generalization to significantly larger problems.

Domain	Train	Validation	Interpolation	Extrapolation
Blocksworld (blocks)	9 (4, 6, 7)	3 (8)	3 (5)	20 (9–17)
Gripper (balls)	4 (2, 4, 6, 8)	2 (9, 10)	3 (3, 5, 7)	16 (12–42, even)
Logistics (goals)	12 (1, 3, 5)	4 (6)	9 (2, 4)	18 (7–15)
VisitAll (cells)	207 (1, 3, 4, 6, 10, 11, 12, 14, 16)	24 (18, 20)	37 (2, 5, 8, 9, 15)	219 (24–121)

add–delete structure, making this domain well-suited for residual state prediction.

Gripper. Gripper models a robot with two grippers transporting balls between rooms. The object set factorizes as $\mathcal{O} = \mathcal{B} \cup \mathcal{R} \cup \{\text{robot}\}$, where \mathcal{B} are balls and \mathcal{R} are rooms. Predicates include $at(x, r)$, $free(g)$, $carry(x, g)$, and $at\text{-}robot(r)$. Operators include MOVE, PICK, and DROP. Although single-step transitions remain sparse, Gripper induces longer causal chains in which object transport must be synchronized with robot motion, creating trajectory-level dependencies not captured by purely local transitions.

Logistics. Logistics is a multi-modal transportation domain with object types $\mathcal{O} = \mathcal{P} \cup \mathcal{T} \cup \mathcal{A} \cup \mathcal{C}$ (packages, trucks, airplanes, cities). Predicates include $at(x, l)$, $in(x, v)$, and $at\text{-}vehicle(v, l)$. Operators include LOAD, UNLOAD, DRIVE, and FLY. Unlike Blocksworld and VisitAll, Logistics induces long-range dependencies across heterogeneous object types and transport layers. Valid plans require coordination across multiple abstraction levels, resulting in deep coupling between distant subgoals. This property severely limits the effectiveness of one-step transition prediction under strict size extrapolation.

VisitAll. VisitAll is a grid navigation domain defined over a lattice of cells $\mathcal{O} = \{(i, j)\}$. Predicates include $at(r, c)$ and $visited(c)$. Operators correspond to unit grid motions that update both at and $visited$. The goal is $g = \bigwedge_{c \in \mathcal{O}} visited(c)$. Although each transition affects only a small number of fluents, the goal conjunct grows linearly with $|\mathcal{O}|$, and the resulting state space grows exponentially. This domain isolates the effect of goal scaling under otherwise simple local dynamics.

Relevance to State-Centric Modeling. All four domains admit deterministic STRIPS semantics with sparse add–delete operators. This ensures that successor states admit a decomposition

$$s_{t+1} = s_t \setminus \text{Del}(a_t) \cup \text{Add}(a_t),$$

which directly motivates our residual transition formulation $\hat{\phi}(s_{t+1}) = \phi(s_t) + \Delta_t$. The domains thus provide a controlled testbed for evaluating whether learned neural approximations $\hat{\gamma}$ can preserve symbolic transition structure under strict size extrapolation.

E Weisfeiler–Leman Graph Embedding Details

This section provides a comprehensive description of the Weisfeiler–Leman (WL) graph embedding procedure used in our state-centric planning framework.

E.1 Background: The WL Algorithm

The Weisfeiler–Leman (WL) algorithm (Weisfeiler and Leman 1968) is an iterative color refinement procedure for graphs. Given a graph $G = (V, E)$ with initial node colors $c^{(0)} : V \rightarrow \Sigma$, the algorithm iteratively refines colors by aggregating neighborhood information:

$$c^{(k+1)}(v) = \text{HASH} \left(c^{(k)}(v), \{ \{ (c^{(k)}(u), \ell(u, v)) \mid u \in \mathcal{N}(v) \} \} \right)$$

where $\mathcal{N}(v)$ denotes the neighbors of v , $\ell(u, v)$ is the edge label, and $\{\{\cdot\}\}$ denotes a multiset. After k iterations, the algorithm produces a multiset of colors $\mathcal{C}^{(k)} = \bigcup_{i=0}^k \{ \{ c^{(i)}(v) \mid v \in V \} \}$.

E.2 Instance Learning Graph Construction

We use the Instance Learning Graph (ILG) representation (Chen, Trevizan, and Thiébaux 2024) to encode planning states. Given a planning instance $\Pi = \langle \mathcal{O}, \mathcal{P}, \mathcal{A}, s, g \rangle$, the ILG $G_{s,g} = (V, E, \mathbf{F}_{\text{cat}}, \mathbf{L})$ is constructed as follows:

Nodes. $V = \mathcal{O} \cup X(s) \cup g$, where:

- \mathcal{O} : object nodes (one per domain object)
- $X(s) = X_p(s) \cup X_n(s)$: state variable nodes (true propositions and numeric fluents)
- g : goal condition nodes

Edges. For each grounded predicate $p = \sigma(o_1, \dots, o_{\text{ar}(\sigma)}) \in X(s) \cup g_p$:

$$E \supseteq \{ (p, o_i) \mid i \in [1, \text{ar}(\sigma)] \}$$

Node Features. Categorical features $\mathbf{F}_{\text{cat}} : V \rightarrow \Sigma_V$ encode node semantics:

$$\mathbf{F}_{\text{cat}}(u) = \begin{cases} \text{object} & \text{if } u \in \mathcal{O} \setminus \mathcal{O}_{\text{const}} \\ u & \text{if } u \in \mathcal{O}_{\text{const}} \\ (\text{pred}(u), \text{apg}) & \text{if } u \in X_p(s) \cap g_p \\ (\text{pred}(u), \text{upg}) & \text{if } u \in g_p \setminus X_p(s) \\ (\text{pred}(u), \text{apn}) & \text{if } u \in X_p(s) \setminus g_p \end{cases}$$

Edge Labels. $L : E \rightarrow \mathbb{N}$ encodes argument position: $L(p, o_i) = i$.

E.3 Feature Extraction

Given the ILG $G_{s,g}$ and k WL iterations, we extract a fixed-dimensional feature vector $\phi(s, g) \in \mathbb{R}^D$ as follows:

1. **Color Refinement:** Run k iterations of WL on $G_{s,g}$, producing color multiset $\mathcal{C}^{(k)}$.
2. **Vocabulary Construction:** During training, collect all unique colors across all training graphs to form vocabulary $\mathcal{V} = \{c_1, \dots, c_D\}$.
3. **Histogram Embedding:** For each graph, compute:

$$\phi(s, g)_i = \text{COUNT}(\mathcal{C}^{(k)}, c_i), \quad i \in [1, D]$$

E.4 Implementation Details

We use the `wlplan` library (Chen 2024) for WL feature extraction with the following configuration:

- **Graph representation:** Instance Learning Graph (ILG)
- **Iterations:** $k = 2$
- **Hash function:** Multiset hash (deterministic)
- **Pruning:** None

Vocabulary Sizes. The resulting vocabulary sizes (feature dimensions D) per domain are:

Domain	Dimension D
Blocksworld	587
Gripper	412
Logistics	723
VisitAll	498

E.5 Properties of WL Embeddings

Permutation Invariance. WL embeddings are invariant to object renaming: for any bijection $\sigma : \mathcal{O} \rightarrow \mathcal{O}$, we have $\phi(\sigma(s), \sigma(g)) = \phi(s, g)$.

Size Invariance. The dimension D depends only on the domain’s predicate structure and training distribution, not on $|\mathcal{O}|$. A model trained on 4-block problems produces embeddings of the same dimension for 100-block problems.

Expressivity. WL embeddings are exactly as expressive as 1-WL message-passing GNNs (Xu et al. 2018): two graphs receive the same embedding if and only if 1-WL cannot distinguish them.

Computational Complexity. For a graph with n nodes, maximum degree δ , and k iterations, the WL algorithm runs in $O(nk\delta)$ time, which is linear in graph size for bounded-degree graphs typical in planning.

F Fixed-Size Factored Encoding Details

While factored representations have been extensively studied in planning (Boutillier, Dearden, and Goldszmidt 2000; Guestrin et al. 2003), our Fixed-Size Factored (FSF) encodings deliberately omit relational structure to serve as a

controlled ablation baseline. FSF represents states as vectors of fixed dimension, where each dimension corresponds to a specific object slot with domain-specific semantics. This design isolates the contribution of permutation and size invariance to generalization by providing a representation that: (i) requires a predetermined maximum object count, (ii) depends on fixed object-to-slot mappings, and (iii) necessitates domain-specific manual design.

F.1 General Structure

FSF encodings have the form $\phi_{\text{FSF}}(s) \in \mathbb{R}^{N+1}$, where N is the maximum number of objects across all problems in the domain. The encoding consists of:

- **Slot 0:** Global/robot state information
- **Slots 1– N :** Per-object state information

Special Values.

- -99.0 : Padding (slot unused for this problem size)
- -10.0 : Don’t-care (goal variable not specified)

F.2 Domain-Specific Semantics

Table 5 provides detailed semantics for each domain.

F.3 Example: Blocksworld Encoding

Consider a 4-block Blocksworld state where:

- Block A is on the table
- Block B is on Block A
- Block C is being held
- Block D is on the table

With object ordering $\{A \mapsto 1, B \mapsto 2, C \mapsto 3, D \mapsto 4\}$:

$$\phi_{\text{FSF}}(s) = [0, \underbrace{0}_{\text{A on table}}, \underbrace{1}_{\text{B on A}}, \underbrace{-1}_{\text{C held}}, \underbrace{0}_{\text{D on table}}, -99, \dots]$$

F.4 Limitations of FSF Encodings

No Size Invariance. FSF encodings require a predetermined maximum object count N . Problems with $|\mathcal{O}| > N$ cannot be represented. This fundamentally limits extrapolation to larger instances.

No Permutation Invariance. FSF encodings depend on a fixed object-to-slot mapping. Different orderings of the same objects yield different vectors, preventing generalization across equivalent states.

Domain-Specific Design. Each domain requires manual design of the encoding semantics, limiting applicability to new domains without expert knowledge.

These limitations motivate the use of WL embeddings, which provide permutation and size invariance without domain-specific engineering.

G Technical Implementation Pipeline

This section describes the complete technical pipeline from symbolic planning instances to trained neural transition models, enabling full reproducibility of our experimental results.

Table 5: Detailed FSF encoding semantics by domain.

Domain	Slot Interpretation	Value Semantics
Blocksworld	Slot 0: Unused (constant 0)	—
	Slot i ($i > 0$): Block i	0 = on table; -1 = held by gripper; $j > 0$ = on block j
Gripper	Slot 0: Robot location	Room index where robot is located
	Slot i (ball): Ball i location	Room index if at room; $-j$ if carried by gripper j
	Slot i (gripper): Gripper i status	0 = free; $j > 0$ = holding ball j
Logistics	Slot 0: Unused (constant 0)	—
	Slot i : Object i (pkg/truck/-plane)	Location index if at location; $-j$ if inside vehicle j
VisitAll	Slot 0: Robot position	Cell index where robot is located
	Slot i ($i > 0$): Cell i	0 = unvisited; 1 = visited

G.1 Data Generation Pipeline

The data generation process transforms raw PDDL domain and problem files into machine-learning-ready state trajectory embeddings through four sequential stages.

Stage 1: Symbolic Plan Generation. We use Fast Downward with a two-tier solving strategy to maximize coverage across problem difficulties. The baseline configuration runs A* search with the landmark-cut admissible heuristic under a 60-second timeout. For problems that exceed this limit, we invoke a fallback configuration using greedy best-first search with the FF heuristic and a 300-second timeout. This staged approach achieves high coverage on training instances (which are intentionally kept small) while maintaining plan quality where possible. Plans are written in standard PDDL action-sequence format.

Stage 2: State Trajectory Reconstruction. Given a valid plan, we reconstruct the complete sequence of intermediate world states using the VAL plan validator in verbose mode. VAL applies each action symbolically and outputs the predicates added or deleted at each timestep. We parse this output to build the full trajectory $\langle s_0, s_1, \dots, s_T \rangle$ where each s_t is represented as a sorted list of ground predicates. This reconstruction is necessary because Fast Downward’s search only maintains heuristic state information, not the explicit symbolic states required for supervised learning. The resulting trajectory files are saved in plain-text format with one state per line.

Stage 3: Weisfeiler-Leman Feature Collection. WL embeddings require a fixed vocabulary collected from the training distribution. For each domain, we parse all training trajectory files and construct instance learning graphs $G_{s,g}$ for every state-goal pair encountered. We run $k = 2$ iterations of color refinement and collect the multiset of final node colors across all training graphs. These color strings are sorted lexicographically and assigned integer indices to form the vocabulary \mathcal{V} . The vocabulary size $D = |\mathcal{V}|$ is domain-dependent but fixed once collected, enabling embeddings of arbitrary test-time problem sizes into \mathbb{R}^D .

Stage 4: Trajectory Embedding. With the vocabulary established, we embed every trajectory across all data splits. For each state s_t in a trajectory, we construct its instance graph $G_{s_t,g}$, perform $k = 2$ WL iterations using the fixed vocabulary \mathcal{V} , and compute the normalized color histogram as the embedding $\phi(s_t) \in \mathbb{R}^D$. Goals are embedded analogously. The resulting trajectory is a matrix of shape $[T, D]$ where T is the plan length, stored as a NumPy array alongside a separate goal vector of shape $[D]$. This compact representation supports efficient batch loading during training.

G.2 Transition Model Training

Dataset Construction for LSTM. The LSTM operates on variable-length sequences. For each problem instance, we load the embedded trajectory matrix $[\phi(s_0), \dots, \phi(s_T)]$ and the goal vector $\phi(g)$. During training, these are collated into padded batches with a custom collate function that tracks the true sequence length of each trajectory. The goal embedding is replicated across all timesteps to form a constant conditioning signal. For delta-mode training, we compute target residuals $\Delta_t = \phi(s_{t+1}) - \phi(s_t)$ on the fly.

Dataset Construction for XGBoost. XGBoost requires flattened tabular input. We extract all consecutive state pairs (s_t, s_{t+1}) from every trajectory and construct feature vectors by concatenating the current state embedding, the goal embedding, and (for delta mode) the difference vector. Concretely, each training example is a row of shape $[2D]$ (concatenated state and goal) with a target vector of shape $[D]$ (next state or delta). This flattening procedure is applied independently to training and validation splits, yielding dense matrices suitable for gradient boosting.

LSTM Architecture and Training. The LSTM model consists of a linear encoder projecting the D -dimensional state and goal vectors into a shared 32-dimensional embedding space. These low-dimensional embeddings are concatenated and fed into a two-layer LSTM with 256 hidden units per layer. The LSTM output is passed through a two-layer feedforward head that projects back to the original D -dimensional space. For state-mode training, we minimize

cosine embedding loss between predictions and targets, encouraging alignment in direction. For delta-mode training, we minimize mean squared error on the residual vectors. We train with the Adam optimizer at a learning rate of 10^{-2} for 250 epochs with early stopping based on validation loss.

XGBoost Architecture and Training. XGBoost is configured for multi-output regression using the squared-error objective. We use histogram-based tree construction on GPU with a maximum tree depth of 8 and a learning rate of 0.1. Training proceeds for up to 1000 boosting rounds with early stopping if validation loss does not improve for 10 consecutive rounds. The model learns an ensemble of regression trees that collectively approximate the mapping from $[\phi(s_t), \phi(g)]$ to $\phi(s_{t+1})$ or Δ_t . The best iteration checkpoint is retained based on validation performance.

Loss Function Selection. For state-mode training, we adopt cosine embedding loss rather than mean squared error. This choice reflects the sparse, high-dimensional nature of WL embeddings: states differing by a single predicate may have Euclidean distances dominated by uninformative dimensions, whereas cosine similarity emphasizes directional alignment in the feature space. Empirically, we observe that cosine loss enables more stable convergence for LSTM models predicting full state vectors. For delta-mode training, we use mean squared error directly on the residual vectors Δ_t , as these deltas are inherently sparse and low-magnitude, making component-wise regression more appropriate than angular alignment. XGBoost uses squared error in both modes as it does not support cosine objectives natively, though the distance metric used during inference (cosine for state mode, Euclidean for delta mode) remains consistent with the training objective’s geometric assumptions.

G.3 Inference and Plan Decoding

Symbolic State Maintenance. During test-time execution, we maintain the current symbolic state s_t explicitly as a set of ground predicates. This state is initialized to the problem’s s_0 and updated only through valid operator applications, ensuring that every intermediate state is well-formed under the domain’s transition function γ .

Neural Successor Prediction. At each planning step, we embed the current symbolic state and goal to obtain $\phi(s_t)$ and $\phi(g)$. These embeddings are passed through the learned transition model to produce either a direct next-state prediction $\hat{\phi}(s_{t+1})$ or a residual prediction Δ_t that is added to $\phi(s_t)$. The resulting target vector \mathbf{v}_t represents the model’s internal prediction of where the plan should transition next.

Symbolic Successor Enumeration. Using the ground operator set \mathcal{A} and applicability preconditions, we enumerate all valid symbolic successors $\text{Succ}(s_t) = \{\gamma(s_t, a) \mid a \in \mathcal{A}, a \text{ applicable in } s_t\}$. Each candidate successor is embedded using the same WL procedure as during training, yielding a set of embedding vectors $\{\phi(s') \mid s' \in \text{Succ}(s_t)\}$.

Nearest Neighbor Decoding. We compute the Euclidean distance (for delta mode) or cosine distance (for state mode)

Table 6: Complete hyperparameter settings for all models.

Parameter	LSTM	XGBoost
<i>Architecture</i>		
Hidden dimension	256	—
Embedding dimension	32	—
Number of layers	2	—
Tree depth	—	8
<i>Training</i>		
Learning rate	10^{-2}	0.1
Batch size	32	—
Max epochs / rounds	250	1000
Early stopping patience	25	10
Optimizer	Adam	—
Loss (state mode)	Cosine	MSE
Loss (delta mode)	MSE	MSE
<i>Inference</i>		
Beam width	3	3
Max planning steps	100	100
Distance metric (state)	Cosine	Cosine
Distance metric (delta)	Euclidean	Euclidean
<i>Model Size</i>		
Parameters	927,602	—
Total tree nodes	—	~ 115,000

between \mathbf{v}_t and each candidate embedding $\phi(s')$. The candidate with minimum distance is selected as the next symbolic state s_{t+1} , and the unique action a satisfying $\gamma(s_t, a) = s_{t+1}$ is appended to the plan. This guarantees that every generated action is applicable and that state evolution respects the symbolic transition semantics.

Termination. Planning terminates when the goal condition $g \subseteq s_t$ is satisfied or when a maximum horizon of 100 steps is reached. The resulting action sequence is validated externally using VAL to confirm correctness.

G.4 Computational Resources

All experiments were conducted on an HPC cluster with the following specifications:

- **GPU:** NVIDIA A100 (40GB VRAM)
- **CUDA Version:** 11.7
- **CPU:** 128 cores per node (for data generation)
- **Memory:** 256GB RAM per node

Total compute time: approximately 1 GPU-hour for all experiments.

G.5 Hyperparameters

Table 6 provides complete hyperparameter settings.